Download is permitted to HPC-Lab members and for educational purposes only

Modeling crack in orthotropic medium using a coupled finite element methods and partition of unity

A. Asadpoure [a], S. Mohammadi [b,*], A. Vafai [a]
[a] *Department of Civil Engineering, Sharif University of Technology, Tehran, Iran.*
[b] *Department of Civil Engineering, University of Tehran, Tehran, Iran.*

Abstract

The problem of modeling crack in orthotropic media is considered. In this field, the extended finite element method has been adopted for modeling the crack and analyzing the domain numerically. In this method, first the finite element model without any discontinuities is created and then the two-dimensional asymptotic crack-tip displacement fields with a discontinuous function are added to enrich the finite element approximation it using the framework of partition of unity. The main advantage is the ability of the method in taking into consideration the crack without any explicit meshing of the crack surfaces, and the growth of a crack can readily be applied without any remeshing. Mixed-mode stress intensity factors (SIFs) are evaluated to determine the fracture properties of domain and compare the results of proposed method with other available numerical or (semi-) analytical methods. The SIFs are obtained by means of the form domain of interaction integral (M-integral).

Keywords: orthotropic media; near-tip displacement; extended finite element method (XFEM); stress intensity factors; crack

Introduction

Orthotropic materials such as composites are widely used in different branches of engineering science. Since the ratio of strength to weight of such materials in many cases is higher than other materials, the applications of these orthotropic materials have been swiftly extended. One of the main applications of such materials is the coating of sensitive structures or making the frameworks of structures. Generally, this material is utilized in thin shell forms, which are very defect susceptible. A major type of defects that most likely to take place in these structures is cracking. Cracks can be initiated under different circumstances such as initial weakness in material strength, fatigue loading, yield loading and imperfection in production procedure. As a result, fracture properties and mechanics of these types of material are highly prominent; reviving the research efforts in this area by great interest.

* Corresponding author. Tel.: +98-21-611-1225-8; fax: +98-21-640-3808.
E-mail address: smoham@ut.ac.ir (S. Mohammadi).

Some analytical investigation have been reported on the fracture behaviour of such materials such as the pioneering one by Muskelishvili [1], Sih et al. [2], Tupholme [3], Viola et al. [4] and more recently Lim et al. [5] and Nobile and Carloni [6].
The analytical solution is not applicable to all problems; in particular to complicated ones. In such cases the numerical solution is the best available tool for resolving the problem. There are many numerical method utilized for modeling cracks in mechanical problems such as the boundary element method (Cruse [7]), the finite element method (Swenson and Ingraffea [8]) and the mesh-less methods such as the element-free Galerkin method (Belytschlo et al. [9]). In many mesh-less methods, simulation of arbitrary geometries and boundaries is so cumbersome. However, the finite element method is more convenient and applicable because of its ability for modeling every boundary conditions, loadings, materials and geometries. But in the finite element model the elements that associated with cracks must be adopted to crack faces. In order to investigate the crack propagation, remeshing techniques are required. To improve these drawbacks and in order to model discontinuities, Blytschko et al. [10] combined FEM with the partition of unity (proposed by Melenk and Babuška [11], Duarte and Oden [12]) soon to be known as the eXtended Finite Element Method (XFEM). In the XFEM, finite element approximation is enriched with appropriate functions extracted from the fracture analysis around the crack-tip. The main advantage of the XFEM is its capability in modeling of discontinuities independently and the mesh is prepared without any consideration about the discontinuities. In 2D isotropic media, Moës et al. [13] and Dolbow et al. [14] proposed an improvement to the work by Blytschko et al. [10]. Sukumar et al. [15] extended the method to three-dimensional problems and Sukumar and prévost [16] proposed the computer implementation.
In this study, a new method is proposed for the second branch of orthotropic materials, as opposed to the one proposed by Asadpoure et al. [18]. In the following sections, first the fundamental formulations of cracked plate are reviewed. Then the XFEM are briefly explained; introducing the enriching functions based on the previous section. In order to verify the formulaton and to investigate the robustness of the proposed method stress intensity factors (SIFs) for cracked media are obtained by the method reported by Kim and Paulino [21] and compared with other numerical or (semi-) analytical methods.

2. Basic and fracture formulation for an orthotropic medium

Consider an orthotropic medium with axes of elastic symmetry co-incident with the Cartesian co-ordinates x-, y- and z-axes. The displacement component along the z-axis and all its derivatives with respect to z are assumed to be zero. The stress-strain equations can be defined as

$$\sigma_x = C_{11}\frac{\partial u}{\partial x} + C_{12}\frac{\partial v}{\partial y} \tag{1.1}$$

$$\sigma_y = C_{12}\frac{\partial u}{\partial x} + C_{22}\frac{\partial v}{\partial y} \tag{1.2}$$

$$\tau_{xy} = C_{66}\left(\frac{\partial u}{\partial y} + \frac{\partial v}{\partial x}\right) \tag{1.3}$$

where C_{ij} (i,j=1,2,6) are the relevant elements of the compliance matrix of the material in x- and y- directions. Now the set of equations for an in-plane elastostatic problem can be expressed as

$$\frac{\partial^2 u}{\partial x^2} + \alpha \frac{\partial^2 u}{\partial y^2} + 2\beta \frac{\partial^2 v}{\partial x \partial y} = 0 \tag{2.1}$$

$$\frac{\partial^2 v}{\partial x^2} + \alpha_1 \frac{\partial^2 v}{\partial y^2} + 2\beta_1 \frac{\partial^2 u}{\partial x \partial y} = 0 \tag{2.2}$$

where

$$\alpha = \frac{C_{66}}{C_{11}}, \quad \alpha_1 = \frac{C_{22}}{C_{66}}, \quad \beta = \frac{C_{12} + C_{66}}{2C_{11}}, \quad \beta_1 = \frac{C_{12} + C_{66}}{2C_{66}} \tag{3}$$

Following the methodology proposed by Viola et al. [4], a transformation is applied in order to express the formulations in term of complex functions. Eqs. (2) can be represent as

$$\frac{\partial \mathbf{\Phi}}{\partial x} + \mathbf{A}\frac{\partial \mathbf{\Phi}}{\partial y} = \mathbf{0} \tag{4}$$

and

$$\mathbf{\Phi} = \left\{ \frac{\partial u}{\partial x}, \frac{\partial u}{\partial y}, \frac{\partial v}{\partial x}, \frac{\partial v}{\partial y} \right\}^T \tag{5}$$

$$\mathbf{A} = \begin{pmatrix} 0 & \alpha & 2\beta & 0 \\ -1 & 0 & 0 & 0 \\ 2\beta_1 & 0 & 0 & \alpha_1 \\ 0 & 0 & -1 & 0 \end{pmatrix} \tag{6}$$

The eigenvalues of the matrix **A** can be obtained by

$$\lambda^4 + 2a_1\lambda^2 + a_2 = 0 \tag{7}$$

where

$$a_1 = \frac{(\alpha + \alpha_1 - 4\beta\beta_1)}{2} \tag{8.1}$$

$$a_2 = \alpha\alpha_1 \tag{8.2}$$

where λ is the eigenvalue of matrix **A**. Regarding above equations, two types of orthotropic material can be found, $a_1 > \sqrt{a_2}$ (type I) and $|a_1| < \sqrt{a_2}$ (type II). In this paper, only type II of the orthotropic materials is studied. The complex functions can be expressed by the following complex variables

$$z_1 = \left(x - \frac{\gamma_1}{\gamma_1^2 + \gamma_2^2} y \right) + i\left(\frac{\gamma_2}{\gamma_1^2 + \gamma_2^2} y \right), \tag{9.1}$$

$$z_2 = \left(x + \frac{\gamma_1}{\gamma_1^2 + \gamma_2^2} y \right) + i\left(\frac{\gamma_2}{\gamma_1^2 + \gamma_2^2} y \right) \tag{9.2}$$

where

$$\gamma_1 = \left[\frac{1}{2}\left(\sqrt{a_2} + a_1 \right) \right]^{1/2} \tag{10.1}$$

$$\gamma_2 = \left[\frac{1}{2} + \left(\sqrt{a_2} - a_1 \right) \right]^{1/2} \tag{10.2}$$

Viola et al. [4] explained the procedure of obtaining the complex variables and functions. Now, consider an infinite orthotropic plate, consisting of a traction free line crack, is subjected to uniform biaxial (T and kT) and shear (S) loads at infinity. Fig. 1 shows the crack geometry, loading conditions and the Cartesian and polar co-ordinates utilized in this study.

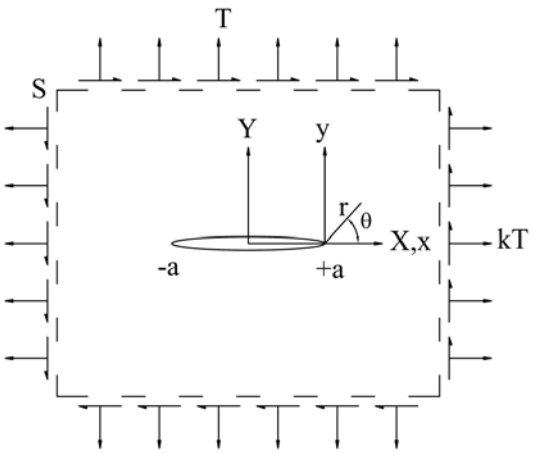

Fig. 1. Crack geometry, loading condition and global and local co-ordinates.

Neglecting the velocity of the velocity of the crack propagation for the present static case, basic solution proposed by Viola et al. [4] results in the following displacement fields in x ad y directions

$$
\begin{aligned}
u &= -2\beta\left[\left(p_3A_1 - p^4B_1 + p_4B_2\right)Y_1 + \left(p_3B_1 + p_4A_1\right)X_1 + p_3B_2X_2\right] \\
&+ \frac{\beta T}{C_{66}D_1}\left\{\left(p_3k_6 + p_4k_5\right)\left[2\left(a + r\cos\theta\right) - \sqrt{2ar}\left(\sqrt{c_1(\theta)}\cos\theta_1/2 + \sqrt{c_2(\theta)}\cos\theta_2/2\right)\right]\right. \\
&\left. - \left(p_3k_5 + p_4k_5\right)\sqrt{2ar}\left(\sqrt{c_1(\theta)}\sin\theta_1/2 - \sqrt{c_2(\theta)}\sin\theta_2/2\right)\right\} \\
&+ \frac{\beta S}{C_{66}D_1}\left\{\left(p_3k_3 + p_4k_4\right)\left[X_1 - X_2 + \sqrt{2ar}\left(\sqrt{c_2(\theta)}\cos\theta_2/2 - \sqrt{c_1(\theta)}\cos\theta_1/2\right)\right]\right. \\
&\left. - \left(p_3k_4 + p_4k_3\right)\left[2Y_1 - \sqrt{2ar}\left(\sqrt{c_1(\theta)}\sin\theta_1/2 + \sqrt{c_2(\theta)}\sin\theta_2/2\right)\right]\right\}
\end{aligned}
\tag{11}
$$

$$
\begin{aligned}
v &= -\left[\left(\gamma_1A_1 - \gamma_2B_1 - \gamma_2B_2\right)Y_1 + \left(\gamma_2A_1 + \gamma_1B_2\right)X_1 - \gamma_1B_2X_2\right] \\
&+ \frac{T}{2C_{66}D_1}\left\{\left(\gamma_1k_6 + \gamma_2k_5\right)\left[\left(X_1 - X_2\right) + \sqrt{2ar}\left(\sqrt{c_1(\theta)}\cos\theta_2/2 - \sqrt{2ar}\cos\theta_2/2\right)\right]\right. \\
&\left. + \left(\gamma_1k_5 - \gamma_2k_6\right)\left[2Y_1 - \sqrt{2ar}\left(\sqrt{c_1(\theta)}\sin\theta_1/2 + \sqrt{c_2(\theta)}\sin\theta_2/2\right)\right]\right\} \\
&+ \frac{S}{2C_{66}D_1}\left\{\left(\gamma_1k_3 - \gamma_2k_4\right)\left[2\left(a + r\cos\theta\right) - \sqrt{2ar}\left(\sqrt{c_1(\theta)}\cos\theta_1/2 + \sqrt{c_2(\theta)}\cos\theta_2/2\right)\right]\right. \\
&\left. + \left(\gamma_2k_3 + \gamma_1k_4\right)\sqrt{2ar}\left(\sqrt{c_1(\theta)}\sin\theta_1/2 + \sqrt{c_2(\theta)}\sin\theta_2/2\right)\right\}
\end{aligned}
\tag{12}
$$

where

$$
p_1 + ip_2 = \frac{\left(\gamma_1 + i\gamma_2\right)}{\alpha + \left(\gamma_1 + i\gamma_2\right)^2}, \qquad p_3 + ip_4 = \left(\gamma_1 + i\gamma_2\right)\left(p_1 - ip_2\right) \tag{13.1}
$$

$$k_1 = \frac{C_{12} - 2\beta p_3 C_{11}}{C_{66}}, \qquad k_2 = 2\beta p_4 \frac{C_{11}}{C_{66}} \tag{13.3}$$

$$k_3 = \frac{C_{22} - 2\beta p_3 C_{12}}{C_{66}}, \qquad k_4 = 2\beta p_4 \frac{C_{12}}{C_{66}} \tag{13.4}$$

$$k_5 = 2\beta p_2 - \gamma_2, \qquad k_6 = 2\beta p_1 - \gamma_1 \tag{13.5}$$

and

$$X_1 = (a + r\cos\theta) - \gamma_1 l^2 r \sin\theta \tag{14.1}$$

$$X_2 = (a + r\cos\theta) + \gamma_1 l^2 r \sin\theta \tag{14.2}$$

$$Y_1 = \gamma_2 l^2 r \sin\theta \tag{14.3}$$

$$A_1 = \frac{(k_3 k - k_1)T}{C_{66}(k_1 k_4 - k_2 k_3)} \tag{14.4}$$

$$B_1 = \frac{S}{2C_{66}k_6} + \frac{T}{2C_{66}k_6}\frac{\left[k(k_4 k_6 - k_3 k_5) + (k_1 k_5 - k_2 k_6)\right]}{(k_1 k_4 - k_2 k_3)} \tag{14.5}$$

$$B_2 = -\frac{S}{2C_{66}k_6} + \frac{T}{2C_{66}k_6}\frac{\left[k(k_4 k_6 - k_3 k_5) - (k_1 k_5 + k_2 k_6)\right]}{(k_1 k_4 - k_2 k_3)} \tag{14.6}$$

$$D_1 = k_3 k_6 - k_4 k_5 \tag{14.7}$$

and

$$c_j(\theta) = \left(\cos^2\theta + l^2 \sin^2\theta + (-1)^j l^2 \sin 2\theta\right)^{1/2}, \quad l^2 = \left(\gamma_1^2 + \gamma_2^2\right)^{-1}, \quad j = 1,2. \tag{15}$$

$$\theta_j = arctg\left(\frac{\gamma_2 l^2 \sin\theta}{\cos\theta + (-1)^j \gamma_1 l^2 \sin\theta}\right), \quad j = 1,2. \tag{16}$$

It is noted that the displacement fields in Eqs. (11-12) are only valid for $\frac{r}{a} < 1$; near the crack-tip.

3. Extended Finite Element Method

The eXtended Finite Element Method (XFEM) was originally proposed by Blytschko and Black [10]. They enriched the finite element approximation by adding some discontinuous functions to the approximation. The procedure of enriching the approximation was performed using the partition of unity method (Melenk and Babuška [11] and Duarate and Oden [12]). For modelling a curved crack, Belytschko and Black [10] separated the crack into a set of straight segments and mapped each one of them into the first segment alignment. For a long curved crack, this procedure becomes very complex. Moës et al. [13] improved the method by introducing the generalized Heaviside function for modeling the crack surfaces. Therefore, the cumbersome mapping procedure is not required and the jump in the displacement (strong discontinuity) around the crack faces (not the crack-tip) would be readily modeled with the new introduced function.
In the extended finite element method, the numerical model is prepared within two parts. In the first part, the mesh is generated without considering the cracks or any discontinuities. Then, with the help of partition of unity method and the discontinuous functions, the FEM mesh is locally enriched in order to capture the effect of cracks or other discontinuities within the mesh. Because of the range of validity of the analytical solution for displacement fields around the crack-tip (in Eqs. (11-12), $\frac{r}{a}<1$), the size of elements containing a crack-tip must be restricted in respect to the crack length and the gradient of stresses around the crack-tip.

3.1 Preliminary equations

For a point **x** locating within a domain, the extended finite element approximation for the enriched displacement field can be defined by

$$\mathbf{u}^h(\mathbf{x}) = \sum_{\substack{I \\ n_I \in \mathbf{N}}} \phi_I(\mathbf{x})\mathbf{u}_I + \sum_{\substack{J \\ n_J \in \mathbf{N}^g}} \phi_J(\mathbf{x})\psi(\mathbf{x})\mathbf{a}_J \qquad (17)$$

where **N** is the set of all nodes in the domain, n_i is the node I, ϕ_I is the shape function associated to node I, $\mathbf{u}_I$ is the vector of regular degrees of nodal freedom in finite element method, $\mathbf{a}_J$ is the added set of degrees of freedom to the standard finite element model, $\mathbf{N}^g$ is the set of nodes that the discontinuity is in its influence (support) domain and $\psi(\mathbf{x})$ is the discontinuous function. Fig. 2 shows the influence domain for node J in an arbitrary discretization of a domain. In Eq. (17), the first expression in the right-hand side is the classical finite element expression to approximate the displacement and second one is the enriched approximation to express the effects of discontinuities in the finite element method.

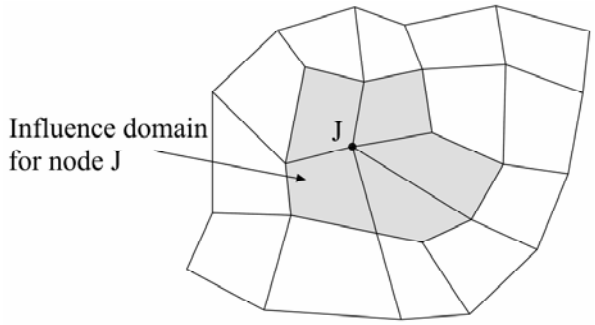

Fig. 2. Influence (support) domain for node J in an arbitrary finite element mesh.

3.2. Modeling crack

For modeling a crack in the extended finite element method, Eq. (17) can be re-written as (Moës et al. [13])

$$\mathbf{u}^h(\mathbf{x}) = \sum_{\substack{I \\ n_I \in \mathbf{N}}} \phi_I(\mathbf{x})\mathbf{u}_I + \sum_{\substack{J \\ n_J \in \mathbf{N}^g}} \mathbf{b}_J \phi_J(\mathbf{x}) H(\mathbf{x}) + \sum_{k \in \mathbf{K}^1} \phi_k(\mathbf{x}) \left(\sum_l \mathbf{c}_k^{l1} F_l^1(\mathbf{x}) \right) + \sum_{k \in \mathbf{K}^2} \phi_k(\mathbf{x}) \left(\sum_l \mathbf{c}_k^{l2} F_l^2(\mathbf{x}) \right) \tag{18}$$

where $\mathbf{b}_J$ is the vector of additional degrees of nodal freedom for modeling crack faces (not crack-tips), $\mathbf{c}_k$ is the vector of additional degrees of nodal freedom for modeling the crack-tips, $\mathbf{N}^g$ is the set of nodes that have crack face (but not crack-tip) in their support domain, $F_l^i(\mathrm{x})$, (i=1,2.), are crack-tip enrichment function and $\mathbf{K}^1$ and $\mathbf{K}^2$ are the sets of nodes associated with crack-tip 1 and 2 in their influence domain, respectively. In Eq. (14), $H(\mathbf{x})$ is the generalized Heaviside function. This function was originally proposed by Moës et al. [13] to model the discontinuity in the displacement in both sides of the crack faces and takes the value +1 if $\mathbf{x}$ is above the crack and –1, otherwise. If $\mathbf{x}^*$ is the nearest point on the crack to $\mathbf{x}$ (see Fig. 3) and $\mathbf{e_n}$ is the unit vector normal to the crack alignment in which $\mathbf{e_s} \times \mathbf{e_n} = \mathbf{e_z}$ ($\mathbf{e_s}$ is the unit tangential vector), then

$$H(\mathbf{x}) = \begin{cases} +1 & ;if\ (\mathbf{x} - \mathbf{x}^*).\mathbf{e_n} > 0 \\ -1 & ;otherwise \end{cases} \tag{19}$$

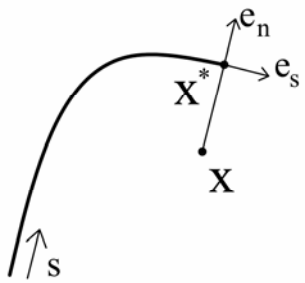

Fig. 3. Unit tangential and normal vectors for Heaviside function.

Fig. 4 illustrates a part of a domain containing a crack with an arbitrary geometry. In this figure, the circled nodes are enriched with Heaviside function and the nodes marked by triangles are enriched with crack-tip function.

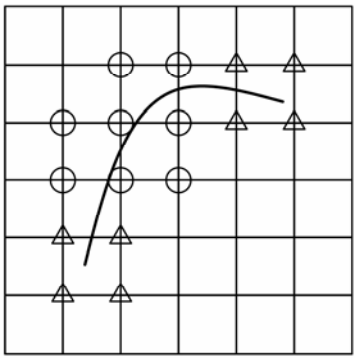

Fig. 4. Node selection for enrichment; the nodes marked by triangles are enriched by crack-tip functions and the circled ones are enriched by the Heaviside function.

The crack-tip enrichment functions are obtained from analytical solution for displacement in the vicinity of the crack-tip. These functions must span the possible displacement space that may be occurred in the analytical solution. Therefore, from Eqs. (11-12), it would be concluded that the functions having preceding properties are as

$$\{F_l(r,\theta)\}_{l=1}^{4} = \left\{\sqrt{r}\cos\frac{\theta_1}{2}\sqrt{g_1(\theta)}, \sqrt{r}\cos\frac{\theta_2}{2}\sqrt{g_2(\theta)}, \sqrt{r}\sin\frac{\theta_1}{2}\sqrt{g_1(\theta)}, \sqrt{r}\sin\frac{\theta_2}{2}\sqrt{g_2(\theta)}\right\} \qquad (20)$$

In Eq. (20), the third and forth functions in the right-hand side of the equation are discontinuous across the crack faces while the others remain continuous. Although, Eq. (20) contains similar terms as to the crack-tip enrichment functions proposed by Asadpoure et. al [18] , fundamentally different definitions are used for the definition of θ_1, θ_1, $g_1(\theta)$ and $g_1(\theta)$ functions.

The discrete system of linear equations in the XFEM in global form can be written as (Sukumar and prévost [16])

$$\mathbf{Kd} = \mathbf{f} \qquad (17)$$

where **K** is the stiffness matrix, **d** is the vector of degrees of nodal freedom (for both classical and enriched ones) and **f** is the vector of external force. The global matrix and vectors are calculated by assembling matrices and vectors of each element. **K** and **f** for each element are defined as

$$\mathbf{k}_{ij}^{e} = \begin{bmatrix} \mathbf{k}_{ij}^{uu} & \mathbf{k}_{ij}^{ua} & \mathbf{k}_{ij}^{ub} \\ \mathbf{k}_{ij}^{au} & \mathbf{k}_{ij}^{aa} & \mathbf{k}_{ij}^{ab} \\ \mathbf{k}_{ij}^{bu} & \mathbf{k}_{ij}^{ba} & \mathbf{k}_{ij}^{bb} \end{bmatrix} \tag{18.1}$$

$$\mathbf{f}_{i}^{e} = \begin{Bmatrix} \mathbf{f}_{i}^{u} & \mathbf{f}_{i}^{a} & \mathbf{f}_{i}^{b1} & \mathbf{f}_{i}^{b2} & \mathbf{f}_{i}^{b3} & \mathbf{f}_{i}^{b4} \end{Bmatrix}^{\mathrm{T}} \tag{18.2}$$

where

$$\mathbf{k}_{ij}^{rs} = \int_{\Omega^{\mathrm{e}}} (\mathbf{B}_{i}^{r})^{\mathrm{T}} \mathbf{D} \mathbf{B}_{j}^{s} \, \mathrm{d}\Omega \quad (r,s = u,a,b) \tag{19.1}$$

$$\mathbf{f}_{i}^{u} = \int_{\partial\Omega_{t}^{h} \cap \partial\Omega^{e}} \varphi_{i} \bar{\mathbf{t}} \, \mathrm{d}\Gamma + \int_{\Omega^{e}} \varphi_{i} \mathbf{b} \, \mathrm{d}\Omega \tag{19.2}$$

$$\mathbf{f}_{i}^{a} = \int_{\partial\Omega_{t}^{h} \cap \partial\Omega^{e}} \varphi_{i} H \bar{\mathbf{t}} \, \mathrm{d}\Gamma + \int_{\Omega^{e}} \varphi_{i} H \mathbf{b} \, \mathrm{d}\Omega \tag{19.3}$$

$$\mathbf{f}_{i}^{b\alpha} = \int_{\partial\Omega_{t}^{h} \cap \partial\Omega^{e}} \varphi_{i} F_{\alpha} \bar{\mathbf{t}} \, \mathrm{d}\Gamma + \int_{\Omega^{e}} \varphi_{i} F_{\alpha} \mathbf{b} \, \mathrm{d}\Omega \quad (\alpha = 1,2,3 \text{ and } 4) \tag{19.4}$$

where Ω^{e} is an element, Ω^{h} is an element such that the crack lies along the edges of that element, $\partial\Omega$ denote the boundary of the domain Ω, $\bar{\mathbf{t}}$ is the traction and **b** is the body force. In Eqs. (19), **B** is the matrix of shape function derivatives,

$$\mathbf{B}_{i}^{u} = \begin{bmatrix} \varphi_{i,x} & 0 \\ 0 & \varphi_{i,y} \\ \varphi_{i,y} & \varphi_{i,x} \end{bmatrix} \tag{20.1}$$

$$\mathbf{B}_{i}^{a} = \begin{bmatrix} (\varphi_{i} H)_{,x} & 0 \\ 0 & (\varphi_{i} H)_{,y} \\ (\varphi_{i} H)_{,y} & (\varphi_{i} H)_{,x} \end{bmatrix} \tag{20.2}$$

$$\mathbf{B}_{i}^{b} = \begin{bmatrix} \mathbf{B}_{i}^{b1} & \mathbf{B}_{i}^{b2} & \mathbf{B}_{i}^{b3} & \mathbf{B}_{i}^{b4} \end{bmatrix} \tag{20.3}$$

$$\mathbf{B}_{i}^{\alpha} = \begin{bmatrix} (\varphi_{i} F_{\alpha})_{,x} & 0 \\ 0 & (\varphi_{i} F_{\alpha})_{,y} \\ (\varphi_{i} F_{\alpha})_{,y} & (\varphi_{i} F_{\alpha})_{,x} \end{bmatrix} \quad (\alpha = 1,2,3 \text{ and } 4) \tag{20.4}$$

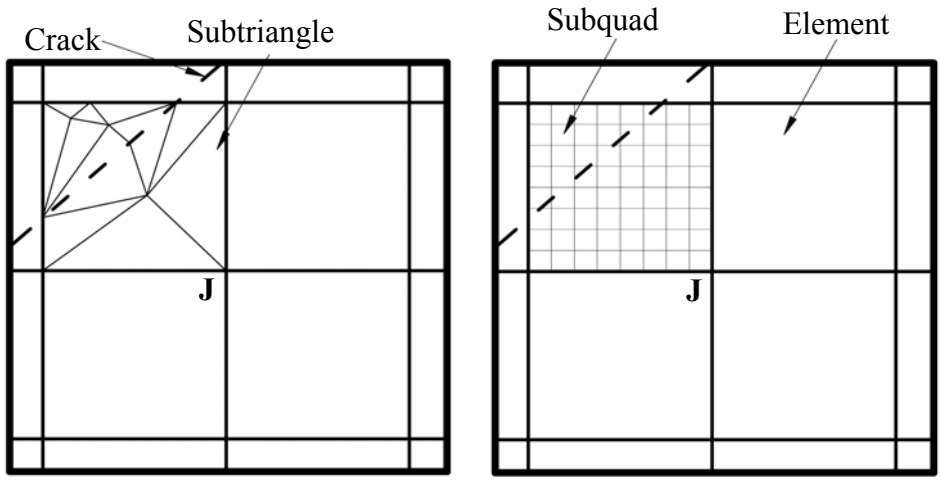

Fig. 5. Two methods for partitioning the cracked element, (a) the cracked element is subdivided into subtriangles, (b) the cracked element is subdivided into subsubquads.

Because the ordinary Gaussian rules do not accurately calculate the integration of enrichment functions in elements cut by a crack, dolbow [14] proposed two methods to overcome this numerical difficalty. The first method is to subdivide the element at both sides of the crack into subtriangles whose edges are adopted to crack faces and the second one is to subdivide the element to subquads. Both methods are illustrated in Fig. 5. In the first method, if the value of $A^-/(A^+ + A^-)$ and $A^+/(A^+ + A^-)$, where A^+ and A^- are the area of the influence domain of a node above and below the crack, respectively (see Fig. 6), are smaller than the tolerance value, that nodes must not be enriched. The tolerance value proposed by Dolbow [14] is 0.01%. In the second method, a node is enriched if there are Gaussian points at both side of the crack in the influence domain of the crack. Fig. 7 shows a mesh that contains a crack while the second method was applied. Although the crack cuts the element in Fig. 7(a), node J must not be enriched because there is no Gaussian point above the crack. In contrary, node J in Fig. 7(b) has to be enriched. In this paper, the second method is utilized.

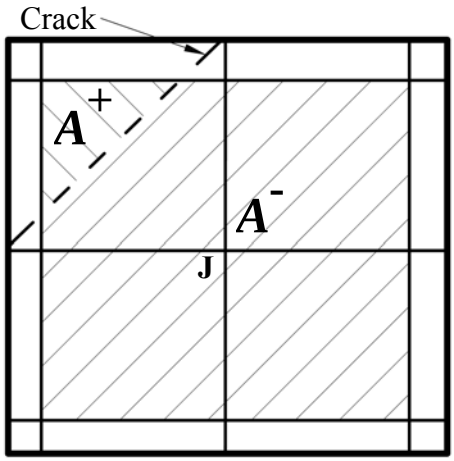

Fig. 6. A^+ and A^- for node J in its influence domain.

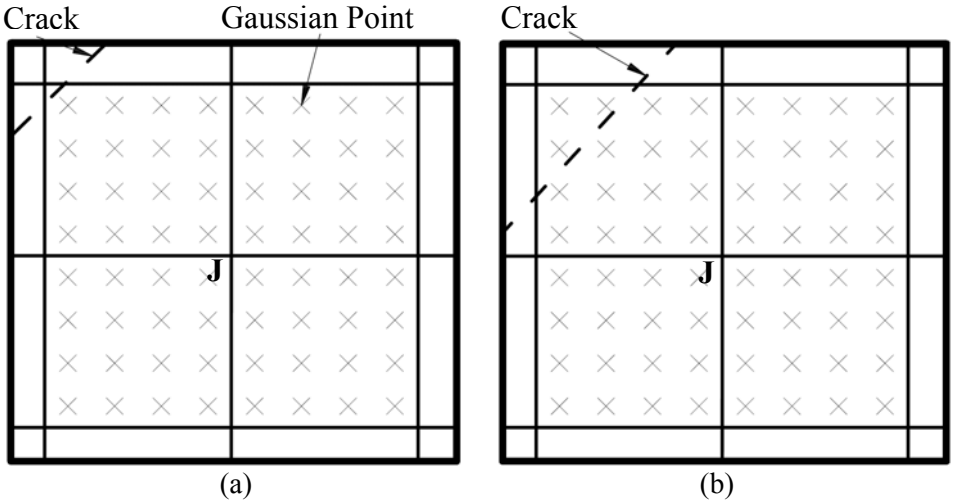

Fig. 7. (a) Node J must not be enriched because in the Gaussian points in its support domain are not present at both side of the crack, (b) node J must be enriched since there are Gaussian points at both sides of the crack.

4. Numerical Examples

In this section some examples are presented. For comparing the results, Stress Intensity Factors (SIFs) and J-integral are calculated and compared. These parameters are among the best parameters for determination of the path of crack propagation. In this section, SIFs and J-integral are obtained by the method proposed by Kim and Paulino [17]. In the subsequent plane stress examples, the following parameters, being the function of independent engineering constants (E_{ij}, ν_{ij}, G_{ij}, i,j=1,2.), would be used

$$E = \sqrt{E_{11}E_{22}}, \quad \nu = \sqrt{\nu_{12}\nu_{21}}, \quad \delta^4 = \frac{E_{11}}{E_{22}} = \frac{\nu_{12}}{\nu_{21}}, \quad \kappa_0 = \frac{E}{2G_{12}} - \nu \tag{21}$$

where E is the efficient Young's modulus, v is the effective Poisson's ratio, δ^4 is the stiffness ratio and κ_0 is the shear parameter.
In the examples, elements containing crack are partitioned into ten subquads and a 2×2 Gaussian rule is utilized for integrations in each ones; however, a 2×2 Gaussian rule is applied in calculating regular finite element parameter.

4.1 Plate with a crack parallel to material axes of orthotropy

In this example, a crack with the same alignment to axes of orthotropy in the center of a plate was studied. At the edges that parallel to the crack, a fixed-grip loading or constant traction is applied. The constant stress is obtained by utilizing a uniform stress (σ=1) and the fixed-grip loading is obtained by applying a load results in the uniform strain (ε_0=1) in the corresponding uncracked plate. The geometry and boundary condition for the problem is illustrated in Fig. 8.

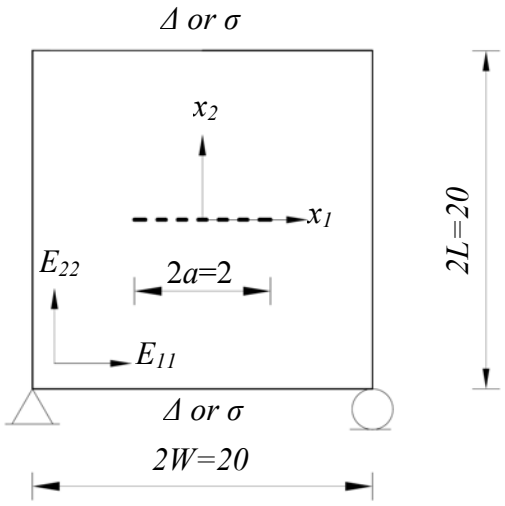

Fig. 8. The geometry and boundary condition for a plate with a crack parallel to material axes of orthotropy

In the FEM discretization, 2116 nodes with 2025 four-noded quadrilateral elements are used (Fig 9). Crack-tip element size is one-sixteenth of the crack length, i.e. $h_e/a = 1/8$. Stress intensity factors are calculated and compared with those reported by Kim and Paulino [17] as shown in table 1.
Table 2 shows the rate of convergence for various integration domain sizes (r_d) for enrichment with and without crack-tip enrichment functions. Numerical results show that when $r_d/a = 0.5$, the values of SIFs are independent from domain size.

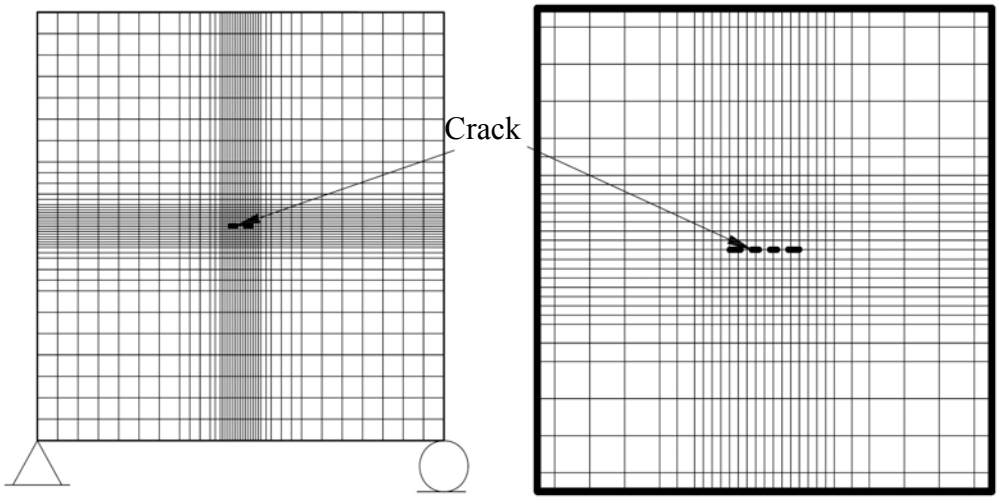

Fig. 9. The discretizated model for a plate with a crack parallel to material axes of orthotropy, (a) whole view of FEM discretization model, (b) the details of descretization around the crack-tip.

Method	$\overline{K_I}$	$\overline{K_{II}}$
Kim and Paulino [17]	0.997	0
Proposed method	1.018	0

Table 1. The values of normalized SIFs for a plate with a crack parallel to material axes of orthotropy, $\overline{K_I} = K_I/\sigma\sqrt{\pi a}$ and $\overline{K_{II}} = K_{II}/\sigma\sqrt{\pi a}$ for the applied uniform stress and $\overline{K_I} = K_I\delta^2/\varepsilon_0 E\sqrt{\pi a}$ and $\overline{K_{II}} = K_{II}\delta^2/\varepsilon_0 E\sqrt{\pi a}$ for fixed-grip loading.

Relative domain size (r_d/a)	**Without crack-tip function**		**Without crack-tip function**	
	$\overline{K_I}$	$\overline{K_{II}}$	$\overline{K_I}$	$\overline{K_{II}}$
0.25	0.966	0	1.018	0
0.5	1.014	0	1.017	0
1	1.015	0	1.017	0
2	1.016	0	1.018	0

Table 2. The rate of convergence of normalized SIFs with and without crack-tip functions for a plate with a crack parallel to material axes of orthotropy; in the table, $\overline{K_I} = K_I/\sigma\sqrt{\pi a}$ and $\overline{K_{II}} = K_{II}/\sigma\sqrt{\pi a}$ for the applied uniform stress and $\overline{K_I} = K_I\delta^2/\varepsilon_0 E\sqrt{\pi a}$ and $\overline{K_{II}} = K_{II}\delta^2/\varepsilon_0 E\sqrt{\pi a}$ for fixed-grip loading.

4.2. Slanted crack

In this example the proposed method is applied to a slanted crack of length 2a located in a finite two-dimensional orthotropic plate under constant applied tension (Fig. 10) where $2a = 2\sqrt{2}$. The angle of the crack with respect to x_1-axis is 45 degrees.

2501 nodes and 40×60 elements are utilized in the FEM discretization (Fig. 11). In the vicinity of the crack, element sizes are smaller than other part of the discretized model and the crack-tip size is one-sixteenth of the crack length.
Stress intensity factors are compared with results reported by Sih et al. [2], Alturi et al. [19], Wang et al. [20] and Kim and Paulino [21]. According to Table 3, the results are different 2.6% for K_I and 3.6% for K_{II} in comparison to Sih et al. [2].

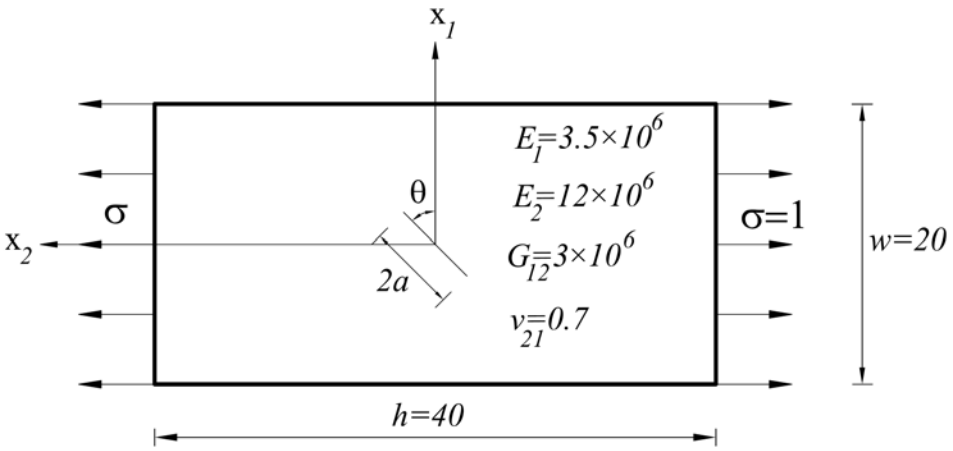

Fig. 10. Geometry of a plate with a slanted crack under remote tension.

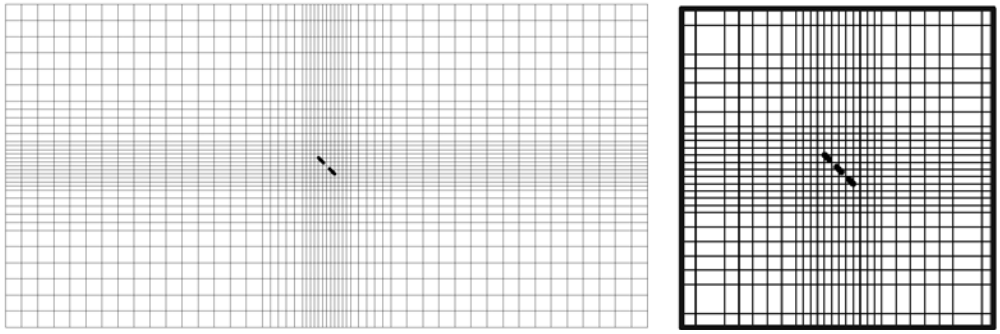

Fig. 11. FEM discretization of a plate with a slanted crack under remote tension, (a) whole view of FEM discretization model, (b) the details of descretization around the crack-tip.

Method		K_I	K_{II}
Sih et al. [2]		1.0539	1.0539
Atluri et al.[19]		1.0195	1.0795
Wang et al.[20]		1.023	1.049
Kim and Paulino [21]	MCC	1.067	1.044
	DCT	1.077	1.035
Proposed method		1.081	1.092

Table 3. SIFs in an orthotropic plate with a slanted crack under uniform remote tension loading

Fig. 12 shows the normalized SIFs corresponding to different crack angle, θ, with respect to x_1-axis. By increasing the crack angle, mode I stress intensity factor reduces; however,

mode II stress intensity factor up to $\theta = 45$ increases, it reaches the maximium value at $\theta = 45$, and then decreases. It is worth noting that for all crack alignment the same discretized model is applied and it shows the capability of XFEM in modeling various crack geometries in the same FEM model.

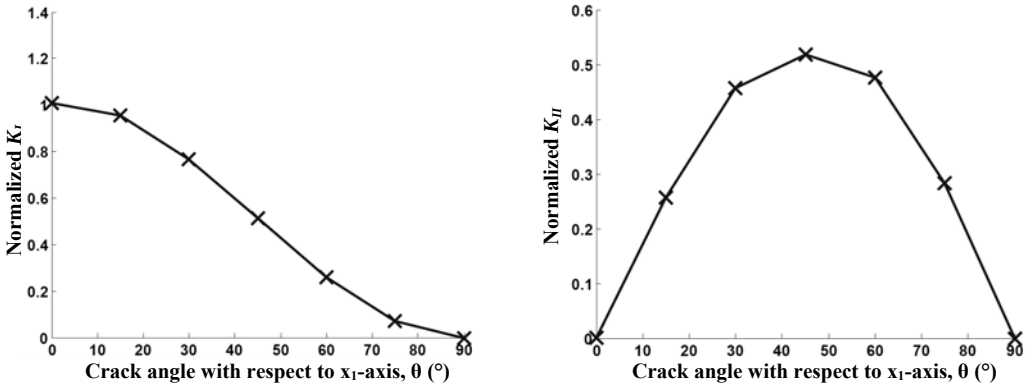

(a) (b)

Fig. 12. The normalized SIFs corresponding to different crack angle of a plate with a slanted crack under remote tension, (a) Normalized SIF for Mode I, (b) Normalized SIF for Mode II. ($\overline{K_I} = K_I/\sigma\sqrt{\pi a}$ and $\overline{K_{II}} = K_{II}/\sigma\sqrt{\pi a}$)

In Fig. 13, the values of SIFs corresponding to different integration domain size are illustrated. In this example, independence domain is obtained when the domain size with respect to crack length is about 0.6.

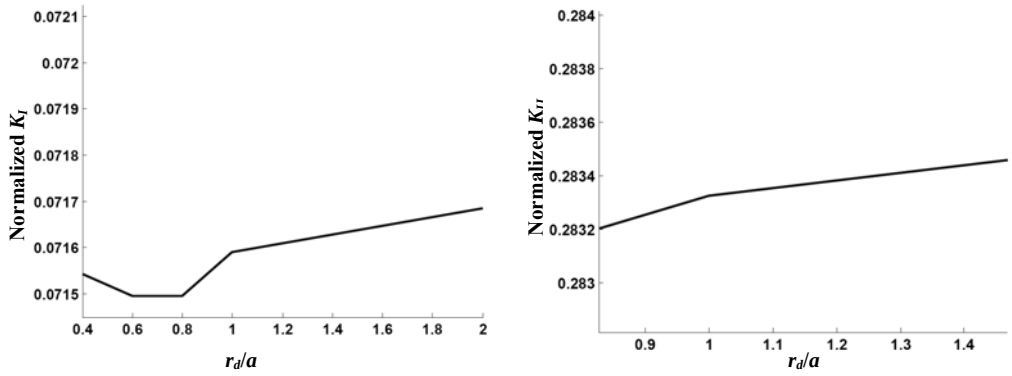

(a) (b)

Fig. 13. The rate of convergence of SIFs with $\theta = 75°$ with respect to relative domain size in a plate with a slanted crack under remote tension, (a) Normalized SIF for Mode I, (b) Normalized SIF for Mode II. ($\overline{K_I} = K_I/\sigma\sqrt{\pi a}$ and $\overline{K_{II}} = K_{II}/\sigma\sqrt{\pi a}$)

4.3. An inclined center crack in a disk subjected to pointed load

The geometry and boundary condition of a disk subjected to pointed load with an inclined crack is shown in Fig. 14. The whole view of FEM discretization is illustrated in Fig. 15 (a), whereas the detail of discretization of around the crack-tips is shown in Fig. 15 (b). 825 four-noded elements with 877 nodes are used in the model. The material axes of

orthotropy were assumed to be parallel to x_1- and x_2-axes and the following material properties were used in the finite element analysis

E_{11}=0.1, E_{22}=1.0, G_{12}=0.5, v_{12}=0.03

Stress intensity factors computed in finite element analysis are compared with those reported by Kim and Paulino [21] for homogeneous orthotropic media. The values of stress intensity factors for both modes in comparison with those ones reported by Kim and Paulino [21] with two methods are shown in Table 4. For mode I, the difference between stress intensity factor of proposed method and Kim and Paulino [21] using M-integral is about 1.7 % and for mode II, slightly increases and reaches to about 2.4 %.
Fig. 16 shows stress intensity factors for another crack inclination between 0° and 45°. The stress intensity factors are decreasing by increasing the crack inclination for mode I, and increasing for mode II. As mentioned in the example 2, only one finite element model is utilized for calculating all crack inclinations.

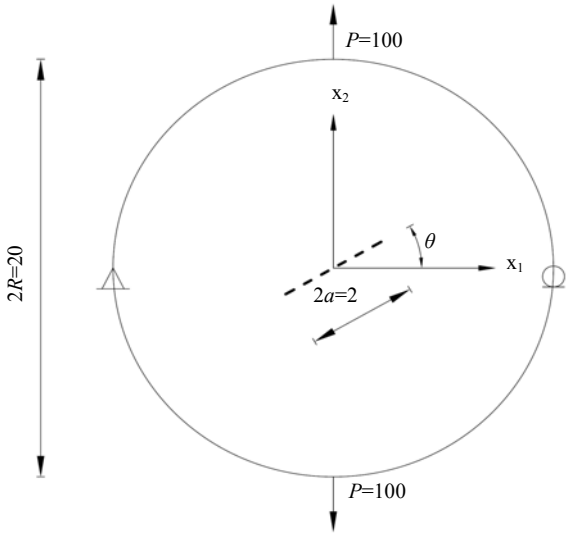

Fig. 14. Geometry and boundary condition for an inclined center crack in a disk subjected to pointed load.

Method		K_I	K_{II}
Kim and Paulino [21]	MCC	16.73	11.33
	M-integral	16.75	11.38
Proposed method		17.03	11.65

Table 4. The values of stress intensity factors for an inclined center crack in a disk subjected to pointed load

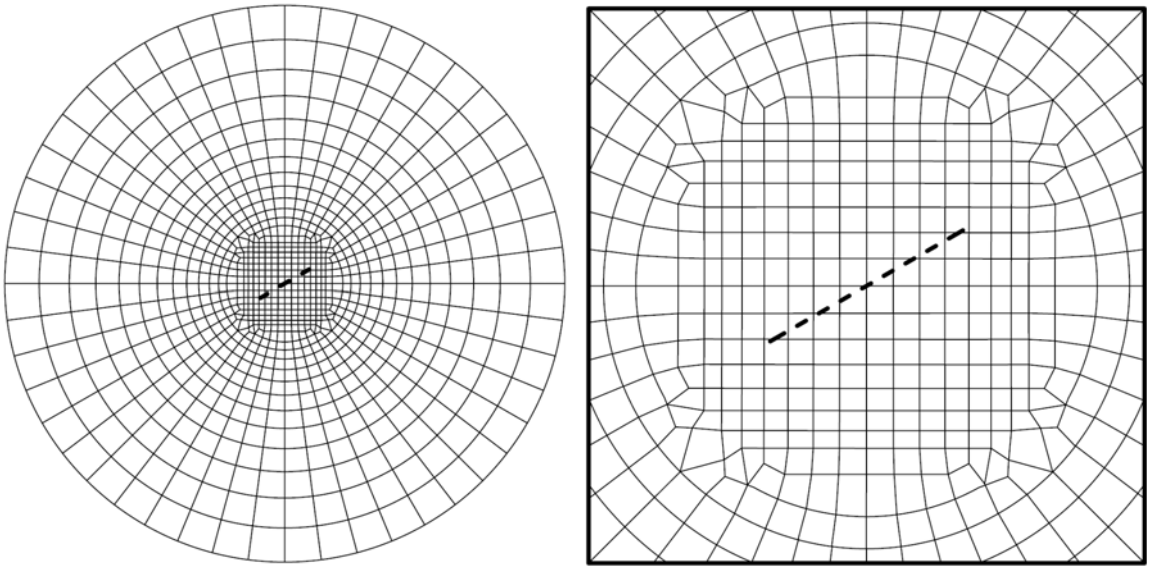

(a) (b)

Fig. 15. FEM discretization for an inclined center crack in a disk subjected to pointed load, (a) whole view of FEM discretization model, (b) the details of descretization around the crack-tip.

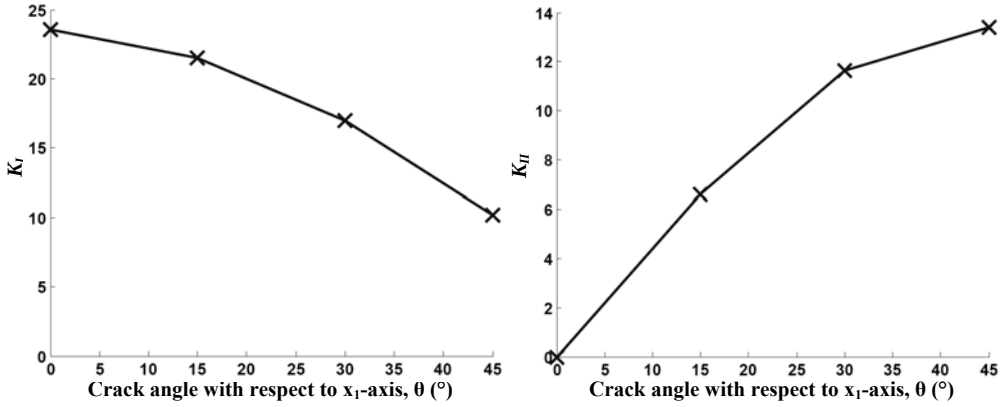

(a) (b)

Fig. 16. The normalized SIFs corresponding to different crack angle of an inclined center crack in a disk subjected to pointed load, (a) SIF for Mode I, (b) SIF for Mode II.

5. Conclusion

The problem of modeling crack in orthotropic media was studied. In this field, the extended finite element method had been adopted for modeling the crack and analyzing

the domain numerically. In the extended finite element method, first the finite element model without any discontinuities is created and then the two-dimensional asymptotic crack-tip displacement fields with a discontinuous function are added to enrich the finite element approximation it using the framework of partition of unity. The main advantage is the ability of the method in taking into consideration the crack without any explicit meshing of the crack surfaces, and the growth of a crack can readily be applied without any remeshing. The analytical solution for displacement is applied to obtain the two-dimensional asymptotic crack-tip functions. The proposed method is considered one group of orthotropic materials. Mixed-mode stress intensity factors (SIFs) were evaluated to determine the fracture properties of domain. The results of proposed method were in good agreement with other available numerical or (semi-) analytical methods.

Reference

[1] N.I. Muskelishvili, Some basic problems on the mathematical theory of elasticity, Noordhoof, Groningen, 1952.
[2] G.C. Sih, P.C. Paris, G.R. Irwin, On cracks in rectilinearly anisotropic bodies. International Journal of Fracture Mechanics 1 (1965), 189–203.
[3] G.E. Tupholme, A study of cracks in orthotropic crystals using dislocations layers. Journal of Engineering and Mathematics 8 (1974), 57–69.
[4] A. Viola, A. Piva, E. Radi, Crack propagation in an orthotropic medium under general loading. Engineering Fracture Mechanics 34(5) (1989), 1155-1174.
[5] W.K. Lim, S.Y. Choi, B.V. Sankar, Biaxial load effects on crack extension in anisotropic solids, Engineering Fracture Mechanics 68 (2001), 403–416.
[6] L. Nobile, C. Carloni, Fracture analysis for orthotropic cracked plates, Composite Structures 68(3) (2005), 285-293.
[7] T. Cruse, Boundary Element Analysis in Computational Fracture Mechanics, Kluwer: Dordrecht, 1988.
[8] D. Swenson, A. Ingraffea, Modeling mixed mode dynamic crack propagation using finite elements: Theory and applications. Comput. Mech. 3 (1988) 381-397.
[9] T. Belytschko, Y.Y. Lu, L. Gu, Element-free Galerkin methods. International Journal for Numerical Methods in Engineering 37 (1994) 229-256.
[10] T. Belytschko, T. Black, Elastic crack growth in finite elements with minimal remeshing, Int, J, Num, Meth, Engng. 45 (1999), 601- 620.
[11] J.M. Melenk, I. Babuška, The partition of unity finite element method: basic theory and applications, Computer Methods in Applied Mechanics and Engineering 139 (1996), 289–314.
[12] C.A. Duarte, J.T. Oden, An H-p adaptive method using clouds, Computer Methods in Applied Mechanics and Engineering 139 (1996), 237–262.
[13] N. Moës, J. Dolbow, T. Belytschko, A finite element method for crack growth without remeshing, International Journal for Numerical Methods in Engineering 46 (1999), 131–150.
[14] J. Dolbow, An Extended Finite Element Method with Discontinuous Enrichment for Applied Mechanics, Theoretical and Applied Mechanics, Northwestern University, Evanston, IL, USA: Ph.D. thesis, 1999.
[15] N. Sukumar, N. Moës, B. Moran, T. Belytschko, Extended finite element method for three-dimensional crack modeling, International Journal for Numerical Methods in Engineering 48 (2000), 1549–1570.
[16] N. Sukumar, J.-H. Prévost, Modeling quasi-static crack growth with the extended finite element method Part I: Computer implementation, Int. J. Solids Structures 40 (2003) 7513-7537.

[17] J.H. Kim, G.H. Paulino, The interaction integral for fracture of orthotropic functionally graded materials: evaluation of stress intensity factors, International Journal of Solids and Structures 40 (2003), 3967-4001.
[18] A. Asadpoure, S. Mohammadi, A. Vafai, Crack analysis in orthotropic media using the extended finite element method, submitted for publication.
[19] S.N. Atluri, A.S. Kobayashi and M.A. Nakagaki, "finite element program for fracture mechanics analysis of composite material". Fract Mech Compos, ASTM STP, 593 (1975), 86–98.
[20] S.S. Wang, J.F. Yau and H.T. Corten, "A mixed mode crack analysis of rectilinear anisotropic solids using conservation laws of elasticity", Int J. Fract, 16 (1980), 247–59.
[21] J.H. Kim and G.H. Paulino, Mixed-mode fracture of orthotropic functionally graded materials using finite elements and the modified crack closure method, Engineering Fracture Mechanics, 69 (2002), 1557–1586.